Med Biol Eng Comput
DOI 10.1007/s11517-009-0437-0

TECHNICAL NOTE

Improving backdrivability in geared rehabilitation robots

Tobias Nef · Peter Lum

Received: 1 October 2008 / Accepted: 3 January 2009

Abstract Many rehabilitation robots use electric motors with gears. The backdrivability of geared drives is poor due to friction. While it is common practice to use velocity measurements to compensate for kinetic friction, breakaway friction usually cannot be compensated for without the use of an additional force sensor that directly measures the interaction force between the human and the robot. Therefore, in robots without force sensors, subjects must overcome a large breakaway torque to initiate user-driven movements, which are important for motor learning. In this technical note, a new methodology to compensate for both kinetic and breakaway friction is presented. The basic strategy is to take advantage of the fact that, for rehabilitation exercises, the direction of the desired motion is often known. By applying the new method to three implementation examples, including drives with gear reduction ratios 100–435, the peak breakaway torque could be reduced by 60–80%.

Keywords Backdrivability · Friction · Breakaway friction · Human–robot interaction · Rehabilitation robotics

T. Nef (✉) · P. Lum
Department of Biomedical Engineering, The Catholic University of America, Washington DC, USA
e-mail: nef@cua.edu

P. Lum
e-mail: lum@cua.edu

T. Nef · P. Lum
Center for Applied Biomechanics and Rehabilitation Research, National Rehabilitation Hospital, Washington DC, USA

1 Introduction

In rehabilitation robotics, particularly in upper limb robotics, the drives must be able to deliver high torques at low velocity. Therefore, many rehabilitation robots are driven by motor-gearbox combinations [2, 10, 11, 14]. In contrast to direct-drive motors, the backdrivability of geared drives is poor due to friction in the gearbox. The back-driving torque τ_b can be defined as the amount of torque the human must apply to the robotic joint in order to perform a user-driven movement. Perfect backdrivability is achieved if $\tau_b = 0$. While admittance controllers perform well with non-backdrivable actuators ($\tau_b \gg 0$), impedance controllers require actuators with good backdrivability ($\tau_b \approx 0$) [6]. In open-loop impedance control, without force/torque sensors, the performance of the controller is directly linked to the drive-backdrivability. Thus, while motor-gearbox drives have adequate power to move the limb, subjects generally must overcome a large τ_b to initiate and to maintain user-driven movements, if no friction compensation is employed. This is problematic since a small τ_b is important for encouraging active participation by the subject during the robot-assisted movement, a critical component of motor learning [3, 8]. Good backdrivability is also desirable for robotic assessment of movement ability.

It is a common practice to use feed-forward control to compensate for gear friction [4, 5]. In a simplified friction model [1], the friction torque τ_f is composed of the velocity-dependent kinetic friction (Coulomb and viscous friction) torque $\tau_{f_k} = f(\omega)$ and a breakaway friction τ_{f_b}. Once the function $f(\omega)$ has been identified, the required motor torque τ_m to compensate for kinetic friction can be estimated based on the velocity measurement and fed to the motor. If the velocity measurement is precise enough and if

Published online: 30 January 2009

$f(\omega)$ has been properly identified, the user will not feel the kinetic friction while he moves the joint. However, with this method, the breakaway friction cannot be compensated, because the user must first overcome τ_{f_b} before motion occurs. Therefore, with state-of-the-art compensation strategies, the user will have to overcome the breakaway torque τ_{f_b} before motion occurs, unless a force/torque sensor is used to directly measure the back-driving torque τ_b. The fundamental problem is that before any motion occurs, it is not known in what direction the user wants to go; therefore it is not possible to compensate for breakaway friction in an open-loop controller since the sign of the compensation torque depends on the direction of the desired movement.

However, in rehabilitation robotics, the direction d of the desired motion is often known. For example, if the exercise is to extend the elbow, then one supporting strategy is to allow the user to move in the direction of extension ($\tau_b = 0$) with very little resistance, at the cost of increasing the resistance to initiation of a flexion movement ($\tau_b > 0$). In this technical note, a new methodology to compensate for both kinetic and breakaway friction is presented. The basic strategy is to assume that the direction d of the desired motion is known and to use this information to compensate for the breakaway friction.

The new method is tested on three implementation examples. For convenience, three motor-gear configurations of the ARMin exoskeleton robot [9, 10] have been used for the experiments. The exoskeleton has been demounted for the experiments, and each configuration has been individually tested. Namely, the exoskeleton's elbow joint, internal/external shoulder rotation and shoulder ab/adduction have been used for these experiments (Table 1).

2 Methods

2.1 Experimental setup

A schematic of the experimental set-up for a single joint is shown in Fig. 1. The human H interacts with the output of the gearbox G_2 through a torque sensor S_2. G_2 is rigidly connected to the output flange of G_1 which is linked via the position sensor S_1 to the motor M. Three different configurations have been selected to evaluate the new methodology as shown in Table 1. Note that the torque sensor S_2 is used for evaluation only and is not part of the compensation algorithm.

Configuration 1 is a Harmonic Drive (HD) gearbox coupled directly with the DC motor. In Configuration 2, the DC motor is connected to the input of the HD gearbox via a belt drive. And in Configuration 3, the DC motor is coupled directly with the HD gearbox, and the output of the gearbox is coupled to the sensor via a belt drive. The motor torque τ_m is not directly measured, but can be derived from the motor current using

$$\tau_m = i_m \cdot k_t \tag{1}$$

where $k_t = 0.119$ Nm/A is the motor's torque constant.

2.2 Friction model

A detailed friction model suitable for industrial controller design is given in [1] as

$$F(\omega) = \left[\alpha_0 + \alpha_1 e^{(-\beta_1|\omega|)} + \alpha_2\left(1 - e^{-\beta_2|\omega|}\right)\right]\mathrm{sgn}(\omega) \tag{2}$$

where Coulomb friction is given by α_0 [Nm], breakaway friction is $(\alpha_0 + \alpha_1)$ [Nm], and α_2 [Nms/rad] represents the

Table 1 Drive chain configurations

	G_2	n_2	G_1	n_1	$n_1 \cdot n_2$	M	ARMin axis [9]
Configuration 1	None	1	HD gearbox[a]	100	100	Maxon Re 35	Upper arm ab/adduction
Configuration 2	HD gearbox[a]	100	Belt drive	1	100	Maxon Re 35	Elbow flexion/extension
Configuration 3	Belt drive	14.5	HD gearbox[b]	30	435	Maxon Re 35	Int./ext. shoulder rotation

[a] HFUC 14HUFC 1:100 gearbox, Harmonic Drive Inc.

[b] HFUC 14HUFC 1:30 gearbox, Harmonic Drive Inc.

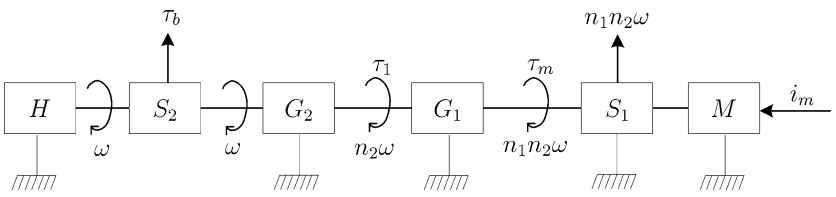

Fig. 1 Experimental setup with DC motor M (RE 35, Maxon Inc.), incremental position encoder S_1 (4000 imp/rot), gearbox $G1$ with the reduction ratio n_1, gearbox G_2 with the ratio n_2, torque sensor S_2 (6 DoF load cell, JR3 Inc.), and the human H. S_2 measures the backdriving torque τ_b

viscous friction model. The kinetic friction is defined as the sum of the first and the last term in (2). The Stribeck effect is modeled with an exponential second term in the model (2). The model given by (2) includes Coulomb friction, viscous friction, static friction, and negative viscous friction. The model is highly nonlinear and discontinuous at zero. In the given friction model, friction depends only on velocity. However, friction can also depend on position, but this dependence is negligible [13] and neglected here.

2.3 Kinetic friction identification

The relationship between the joint angular velocity ω and the kinetic friction torque τ_{f_k} is identified by driving the joint with a constant velocity ω_c and measuring the required motor current i_m. The reference velocity ω_{ref} is selected such that the joint position φ does not exceed the range of motion (ROM) of the joint. Consequently, a piecewise linear velocity profile is selected for the reference signal ω_{ref} of the joint-velocity controller. It is

$$\omega_{ref} = \begin{cases} \alpha \cdot t & \text{for } 0 \le t \le 0.1\,T \\ \omega_c & \text{for } 0.1T < t \le 0.4\,T \\ \omega_c - \alpha \cdot (t - 0.4\,T) & \text{for } 0.4T < t \le 0.6\,T \\ -\omega_c & \text{for } 0.6T < t \le 0.9\,T \\ -\omega_c + \alpha \cdot (t - 0.9T) & \text{for } 0.9 < t \le T \end{cases} \quad (3)$$

where $\alpha = 10\ \omega_c/T$ is the angular acceleration and T is the cycle duration that depends on the ROM of the joint under investigation. It is

$$\varphi_{max} - \varphi_{min} = \int_{t=0}^{t=0.5\,T} \omega_{ref}\ \mathrm{d}t = \frac{4}{10} \cdot \omega_c \cdot T \quad (4)$$

and

$$T = \frac{10 \cdot (\varphi_{max} - \varphi_{min})}{4 \cdot \omega_c} \quad \text{with } -100^\circ/\mathrm{s} \le \omega_c \le 100^\circ/\mathrm{s}. \quad (5)$$

The mean motor current $\overline{i_m}$ is determined by averaging the motor current i_m current during the constant velocity phases. The result from this procedure is a look-up table, that describes the function $f(\omega)$ which maps angular velocities to current.

For feed-forward compensation, it is desirable to convert the look-up table into a continuous function. The friction model (2) is not continuous at zero, which can cause stability problems [13]. Therefore, a combination of a sigmoid and a linear function is selected to fit the measured data [12]. Sigmoid functions are continuous and strictly monotonically increasing. The general form is

$$i_m = \hat{f}(\omega) = c_6 \cdot \omega + \frac{c_1 \cdot \mathrm{e}^{c_2\omega} - c_3}{c_4 \cdot \mathrm{e}^{c_2\omega} + c_5}. \quad (6)$$

The coefficients $c_1 \ldots c_6$ are selected by numerical minimization [7] with the objective to minimize the error E with

$$E = \sum_{\omega=-100^\circ/\mathrm{s}}^{\omega=+100^\circ/\mathrm{s}} \left| \mathrm{f}(\omega) - \hat{\mathrm{f}}(\omega) \right|. \quad (7)$$

The resulting coefficients are introduced into (6) and the resulting function $\hat{f}(\omega)$ is then used for Coulomb friction compensation.

2.4 Breakaway friction identification

The breakaway friction is identified by measuring the breakaway current i_b required to start the motor. Thus, the current ramp $i_m = g(t)$ as described by Eq. 8 is applied to the motor. In the meantime, the joint velocity ω and the motor current i_m are measured and recorded:

$$i_m(t) = \begin{cases} s \cdot t & \text{for } 0 < t \le 0.4T \\ 0 & \text{for } 0.4T < t \le 0.5T \\ -s \cdot (t - 0.5T) & \text{for } 0.5T < t \le 0.9T \\ 0 & \text{for } 0.9T < t \le 1T \end{cases} \quad (8)$$

where s is the gradient of the current ramp and T is the cycle time. The rotor will not turn until the torque produced by the motor is big enough to overcome the breakaway friction. Therefore, the breakaway current i_b is defined as the value of the actual motor current i_m at time t_s when the motor brakes free (Fig. 2). Two breakaway currents are measured: i_{b_p} for rotations in the positive direction, and i_{b_n} for rotations in the negative direction. These values are determined using the following criteria:

$$i_{b_p} = i_m \quad \text{if } \omega(t_{s_p}) > 0 \quad \text{and } \omega(t_{s_p} - \Delta t) = 0 \quad (9)$$

and

$$i_{b_n} = i_m \quad \text{if } \omega(t_{s_n}) < 0 \quad \text{and } \omega(t_{s_n} - \Delta t) = 0, \quad (10)$$

with $\Delta t = 1$ ms equal to the system's sample time.

The measurement cycle is repeated 200 times for each motor/gear combination and the mean values $\overline{i_{b_p}}$ and $\overline{i_{b_n}}$ are calculated. If the friction behavior of the drive is symmetric, then the magnitude of the breakaway currents are similar, thus $\overline{i_{b_p}} = -\overline{i_{b_n}} = \overline{i_b}$. The values for s and T must be selected such that the current ramp is slow enough, in order to avoid the influence of motor and current converter dynamics. The selected values for s are 0.05, 0.06, 0.12 A/s for Configuration 1–3 and the selected value for T is 10 s for all configurations.

2.5 Friction compensation

The current i_{f_k} required to compensate for the kinetic friction is calculated using Eq. 6. The current for

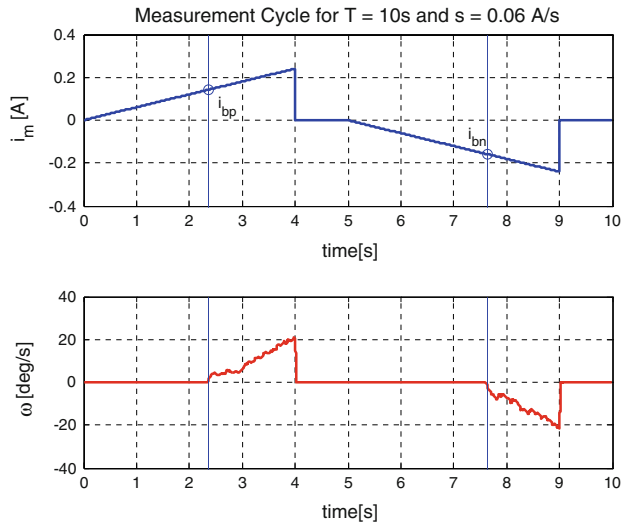

Fig. 2 Breakaway friction identification procedure for Configuration 2 with the parameters $s = 0.06$ A/s and $T = 10$ s. The graph shows the motor current i_m and the angular velocity ω. The vertical lines indicate the point in time when the rotor starts to turn ($t_\mathrm{bp} \approx 2.35$ s, $t_\mathrm{bn} \approx 7.6$ s) and when the breakaway currents $i_{\mathrm{b_p}}$ and $i_{\mathrm{b_n}}$ are captured. This procedure is repeated 200 times for each configuration

breakaway friction compensation $i_{\mathrm{f_b}}$ is different from zero only at zero velocity. Depending on the direction d it is either $i_{\mathrm{f_b}} = +0.9 \cdot \overline{i_\mathrm{b}}$ or $i_{\mathrm{f_b}} = -0.9 \cdot \overline{i_\mathrm{b}}$. The factor 0.9 is introduced to prevent the robot from starting unintentionally.

Figure 3 shows the block diagram of the compensation algorithm. The input d is 1 if the desired movement goes in the positive direction, and -1 for the negative direction. If $d = 0$, the breakaway friction compensation is disabled and only kinetic friction is compensated.

2.6 Experimental evaluation

The ARMin exoskeleton robot [9, 10] has been demounted for the experiments. The motor/gear units of three joints (Table 1) have been individually examined in an orientation where gravity has no effect. To evaluate the new methodology, two cases are compared for all three joint configurations. Case 1 is with kinetic friction compensation only ($d = 0$) and case 2 is with kinetic and breakaway friction compensation ($d = \pm 1$). These cases are compared for a reference movement that includes constant velocity phases, acceleration phases and standstill; once in the positive, and once in the negative direction (Fig. 5, top).

In order to assure consistency of movements between the two cases, a graphical display is used to present the reference movement to the human. The human has to repeat the reference movement ten times, while the back-driving torque τ_b is measured and recorded. Afterwards, the individual trials are synchronized and ensemble averaged over the ten repetitions.

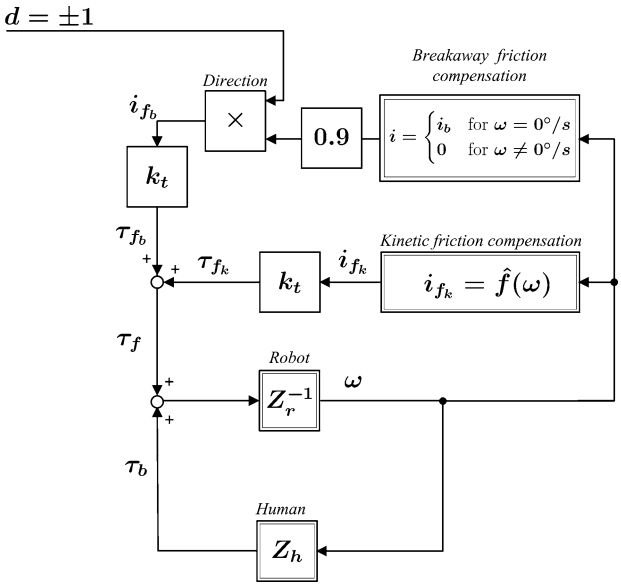

Fig. 3 Block diagram of the friction compensation. The robot Z_r^{-1} is represented as admittance and is composed of the motor M and the gearboxes G_1 and G_2. The velocity output ω is input to the impedance Z_h representing the human who is exerting the torque τ_b onto the robot. The velocity signal ω is obtained by differentiating the position φ and serves as input for both, the kinetic friction compensation and the breakaway friction compensation blocks. The constant k_t is the motor's torque constant

3 Results

The kinetic and breakaway frictions have been identified for all three configurations (Fig. 4). The motor current i_m required to overcome friction depends on the gear configuration. Configuration 1 (Motor-HD, 1:100) has the lowest friction. Configuration 2 (Motor-Belt-HD, 1:100) is characterized by a higher amount of friction, especially for higher velocities. Configuration 3 (Motor-HD-Belt, 1:435) has by far the highest amount of fiction.

The values and standard deviations for the breakaway currents to overcome breakaway friction are $i_\mathrm{b1} = 99.5$ mA $\pm$ 3.4 mA, $i_\mathrm{b2} = 137.7$ mA $\pm$ 4.3 mA and $i_\mathrm{b3} = 335.7$ mA $\pm$ 17.2 mA. The approximations for the dynamic friction have the general form (6) and are for the three configurations

$$i_{\mathrm{m}_{1\ldots3}} = \hat{f}_{1\ldots3}(\omega) = c_6 \cdot \omega + \frac{c_1 \cdot \mathrm{e}^{c_2\omega} - c_3}{c_4 \cdot \mathrm{e}^{c_2\omega} + c_5} \quad \text{with } c_{1\ldots6}$$
$$= \begin{cases} 0.1101, 1.2456, 0.1359, 1.1671, 1.4959, 0.0008\,(\text{conf.1}) \\ 0.8896, 3.0735, 0.3082, 2.4381, 0.8727, 0.0032\,(\text{conf.2}) \\ 0.3629, 1.1022, 0.3000, 2.2795, 1.8775, 0.0027\,(\text{conf.3}) \end{cases} \tag{11}$$

The results of the experimental evaluation are presented in Fig. 5. For each configuration, a test person repeated the same movement pattern ten times with breakaway friction compensation off ($d = 0$) and ten times with breakaway

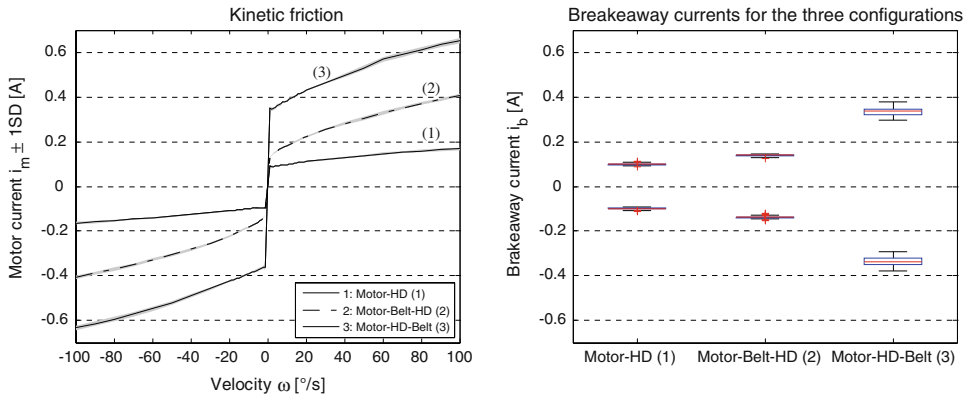

Fig. 4 Kinetic and breakaway friction for the three configurations. The kinetic friction has been identified by measuring the motor current i_m that is required to drive the motor at the given velocity ω. To determine the breakaway friction, a slow current ramp has been applied to the motor and the breakaway current i_b has been captured when the rotor started to turn. For all three configurations, i_b corresponded closely to the kinetic friction values at near zero velocity

friction compensation on ($d = \pm 1$). The backdriving torque profiles τ_{b1}, τ_{b2}, and τ_{b3} have been recorded, ensemble averaged over the ten repetitions, and represented for a movement sequence in the positive and for a movement sequence in the negative direction. The backdriving torques τ_b have their maximum at $t \approx 3.5$ s. This is when the human initiates the movement and when he must overcome the breakaway friction. Nevertheless, with the new breakaway friction compensation, the peak value of $|\tau_b|$ is reduced by 60% for Configuration 1, 65% for Configuration 2, and 80% for Configuration 3. Without breakaway friction compensation, the interaction torque during movement initiation is much greater than during constant velocity; but when breakaway friction compensation is added, the torque levels required to initiate movement are only marginally larger than that required during constant velocity. Furthermore, the test subject reported that the breakaway friction compensation made it much easier to perform the desired motion. The peak torque values $|\tau_b|$ required to initiate the movement without breakaway friction compensation are 0.98, 1.28, 6.02 Nm for the three configurations. With the breakaway friction compensation, these values are reduced to 0.39, 0.44, and 1.21 Nm.

4 Discussion and conclusion

The new methodology to improve backdrivability of geared drives by compensation for breakaway friction was effective. The achieved reduction in backdriving torque is important, especially for Configuration 3, which has the largest overall speed reduction ratio of 435. In this configuration, the torque required to initiate movement decreased from 6.02 to 1.21 Nm when the breakaway friction compensation algorithm was implemented. The reduction is achieved without the use of a force/torque sensor and the methodology is ready to be implemented in rehabilitation robots.

The disadvantage of this method is that the direction of the desired movement must be known. While this limits the application to rehabilitation exercises where the desired movement is known, this still represents a large portion of the therapeutic exercises used on many rehabilitation robots. For example, a common technique is to allow the therapist to prescribe a specific movement trajectory using a teach-and-replay mode [10]. During training, the subject contributes as much to the movement as possible and the robot assists as needed to guarantee completion of the movement. Use of this algorithm would be appropriate for this type of robot therapy.

Sigmoid functions have been used to model the friction data. The advantage of sigmoid functions is that they are continuous. The disadvantage is that the Stribeck effect cannot be included in the model. Since the Stribeck effect is very small in the joints under investigation (Fig. 4) this approach is valid. However, for motor/gear units with high Stribeck effects, use of another model [1] might be beneficial. Furthermore, it is known that the friction properties of the gears and the motor's torque constant $k_t = 0.119$ Nm/A change with temperature and wear. Therefore, perfect compensation cannot be achieved. Nevertheless, since calibration involves simply moving the robot joints through a series of rotations using a PD feedback controller, it is possible to recalibrate the algorithms repeatedly at regular intervals to compensate for wear. Short-term temperature effects will vary depending on the work-load and the design of the robot, but it was found that continuous movement of the joints of ARMin [1] for 1 h had only minor effects on the friction characteristics.

Overall, this methodology can be used to improve the backdrivability of geared rehabilitation robots without

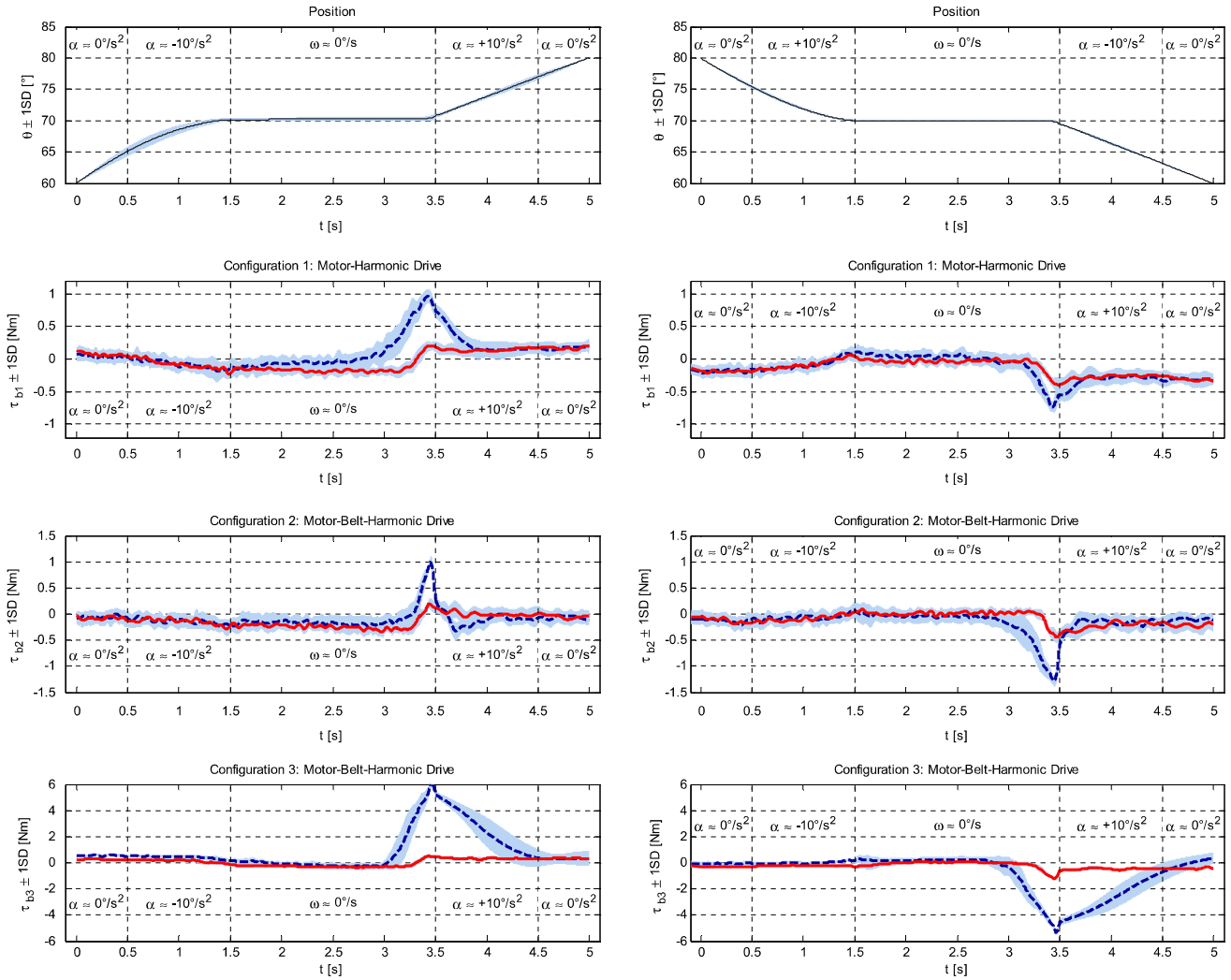

Fig. 5 Results of the experimental evaluation. All lines represent the average and standard deviation of ten movements. The first row shows the trajectories and the other plots show the interaction torque τ_b, with and without breakaway friction compensation. The maximal torque values are observed at $t \approx 3.5$ s when the movement is initiated by the user

force sensors. Future work will be directed toward extending the algorithm to allow user control of movement direction. This can be achieved with the use of inexpensive sensors to detect the onset and direction of a movement attempt. In addition, work is underway to incorporate the friction algorithm into multijoint movement patterns, where reversals at some joints may be a desired component of the trained movement.

References

1. Canudas de Wit C, Noel P, Aubin A, Brogliato B (1991) Adaptive friction compensation in robot manipulators: low velocities. Int J Robot Res 10(3):189–199. doi:10.1177/027836499101000301
2. Carignan C, Liszka M, Roderick S (2005) Design of an arm exoskeleton with scapula motion for shoulder rehabilitation. In: Proceedings of the 12th IEEE international conference on advanced robotics ICAR, July 18–20, Seattle, pp 524–531. doi:10.1109/ICAR.2005.1507459
3. Dromerick AW, Lum PS, Hidler J (2006) Activity-based therapies. NeuroRX 3(4):428–438. doi:10.1016/j.nurx.2006.07.004
4. Hauschild JP, Heppler GR (2007) Control of harmonic drive motor actuated flexible linkages. In: IEEE international conference on robotics and automation, 10–14 April, Rome, pp 3451–3456. doi: 10.1109/ROBOT.2007.364006
5. Kermani MR, Patel RV, Moallem M (2007) Friction identification and compensation in robotic manipulators. IEEE Trans Instrum Meas 56(6):2346–2353. doi:10.1109/TIM.2007.907957
6. Krebs HI, Ferraro M, Buerger SP, Newbery MJ, Makiyama A, Sandmann M, Lynch D, Volpe BT, Hogan N (2004) Rehabilitation robotics: pilot trial of a spatial extension for MIT-manus. J Neuroeng Rehabil 1:5. doi:10.1186/1743-0003-1-5
7. Lagarias JC, Reeds JA, Wright MH, Wright PE (1998) Convergence properties of the Nelder-Mead simplex method in low dimensions. SIAM J Optim 9(1):112–147
8. Lotze M, Braun C, Birbaumer N, Anders S, Cohen L (2003) Motor learning elicited by voluntary drive. Brain 126(4):866–872. doi:10.1093/brain/awg079

9. Nef T, Riener R (2008) Shoulder actuation mechanisms for arm rehabilitation exoskeletons. In: Proceedings of the second IEEE/RAS-EMBS international conference on biomedical robotics and biomechatronics, October 19–22, Scottsdale
10. Nef T, Mihelj M, Riener R (2007) ARMin—a robot for patient-cooperative arm therapy. Med Biol Eng Comput 45(9):887–900. doi:10.1007/s11517-007-0226-6
11. Rosen J, Perry JC, Manning N, Burns S, Hannaford B (2005) The human arm kinematics and dynamics during daily activities—toward a 7 DOF upper limb powered exoskeleton. In: Proceedings of the 12th IEEE international conference on advanced robotics ICAR, July 18–20, USA, pp 532–539. doi:10.1109/ICAR.2005.1507460
12. Selmic RR, Lewis FL (2000) Deadzone compensation in motion control systems using neural networks. IEEE Trans Autom Control 45(4):602–613. doi:10.1109/9.847098
13. Selmic RR, Lewis FL (2002) Neural-network approximation of piecewise continuous functions: application to friction compensation. IEEE Trans Neural Netw 13(3):745–751. doi:10.1109/TNN.2002.1000141
14. Zhang LQ, Park HS, Ren Y (2007) Developing an intelligent robotic arm for stroke rehabilitation. In: Proceedings of the 10th IEEE international conference on rehabilitation robotics ICORR, June 12–15, Noordwijk, pp 984–993. doi:10.1109/ICORR.2007.4428543